JOURNAL OF COMPUTATIONAL PHYSICS 109, 289–305 (1993)

Matched Asymptotic Solutions of Impulsive Flow over an Elliptic Cylinder

HAMID JAFROUDI AND HSUN-TIAO YANG

Department of Aerospace Engineering, University of Southern California, Los Angeles, California 90089-1191

AND

JERRY HERMEL

Hughes Aircraft Company, Los Angeles, California 90009

Received September 11, 1991; revised September 15, 1992

The initial flow field of an impulsively started incompressible viscous flow over an elliptic cylinder is analyzed by the method of matched asymptotic expansions. Analytical solutions for the outer and inner flow fields are obtained to the third order. The Symbolic Manipulation Program is used to facilitate the work. Flow separation is studied in some detail, as are the surface quantities such as the vorticity, the pressure distribution, the drag, and the lift coefficients.

1. INTRODUCTION

To investigate the generation of the viscous layer, its growth, separation, and resulting effect on the flow field over an elliptic cylinder, Wang [12] was the first to obtain a second-order analytic solution by the method of asymptotic expansions. It is to be noted Wang called his solution first-order, but in conventional notation it should be called second-order. His Fig. 2 shows the movement of the separation point along the ellipse perimeter for six angles of attack at Reynolds number 100, where the Reynolds number is defined in terms of one-half of the mean of the major and minor axes. The six curves there are continuous, smooth, and well behaved. Billings [2] generalized Wang's work by adding rotation to the elliptic cylinder and he recovered Wang's solution without rotation. However, Billings' Fig. 9 for angle of attack 25°, Reynolds number 1000, shows a discontinuity in the separation–reattachment curve at the surface location $\eta = 25°$ ($\eta = 155°$ in our notation). This behavior was apparently missed by Wang. See Fig. 1, in which Wang's curve for a 2:1 ellipse at angle of attack 36°, $\mathrm{Re} = 100$ was read from his Fig. 2 and reproduced as open circle points. Note that his curve is continuous and the present result (to second order) depicted by the solid curve is discontinuous at $\eta = \pi - \alpha = 144°$. In the meantime, Hermel [6] extended Wang's work to third order, paralleling the work of Barlev and Yang [1] for the circular cylinder. Hermel obtained essentially the same result as Billings.

In the present work, we redeveloped the analytic solutions of the second and then third order, with the third-order results different from previous studies. When the angle of attack is 0° or 90°, the initial flow being symmetric, the separation time versus surface angle η curve is well behaved as in Wang's original work. When the angle of attack α is other than 0° or 90°, there is a discontinuity at the surface location $\eta = \pi - \alpha$. The left branch goes to infinity while the right branch goes to zero. This may be attributed to the concept of symmetry paradoxes, i.e., almost-symmetric causes may have quite nonsymmetric consequences. In our computation the discontinuity begins to appear at an angle of attack greater than 0°, say 1°. See Birkhoff [3] and Goldshtik [5]. The progression of flow separation with time is further discussed in Section 6.3.

In addition to the second-order solutions by Wang and then by Billings, it is important to obtain third-order solutions for the following reasons:

1. Within the framework of the first- and second-order solutions, the normal pressure gradient across the viscous layer remains zero as in conventional boundary layer theory. In the third-order solution, this is no longer the case.

2. Up to the second-order solutions, the separation bubble as sketched in Fig. 5 of Wang does not appear at all. This is because the streamline pattern is plotted from the second-order composite solution of the stream function.

0021-9991/93 $5.00

581/109/2-10

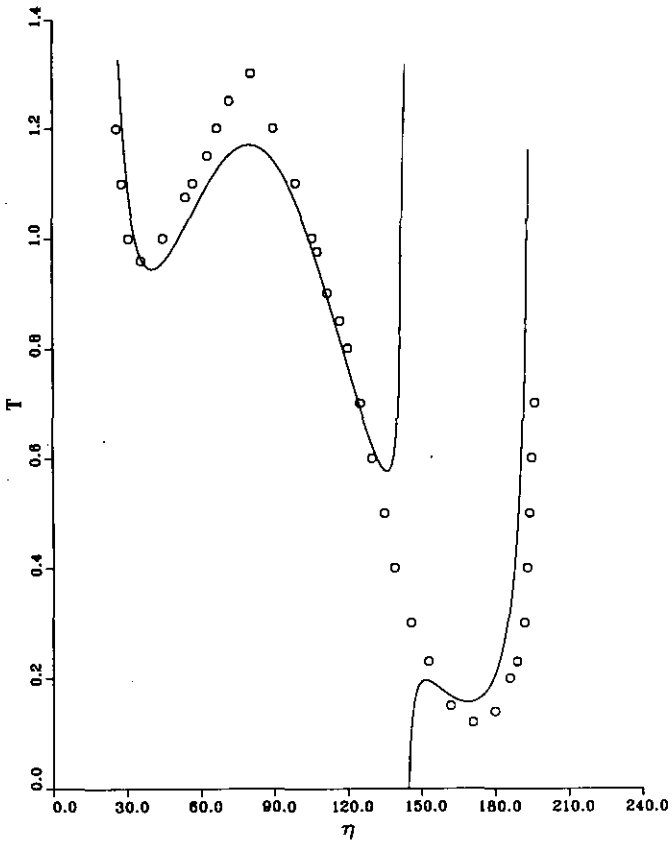

FIG. 1. Movement of separation and reattachment points for a 2:1 ellipse at angle of attack 36°; ○, Wang [12].

That solution is composed of the second-order outer solution plus the first-order inner solution minus the common part. However, the first-order inner solution does not predict flow separation. On the other hand, the third-order composite solution consists of the third-order outer solution and the second-order inner solution which does predict flow separation and hence the appearance of separation bubbles.

3. Once the first-, second-, and third-order solutions are obtained, we then have enough terms to improve the asymptotic series by the Padé approximant or Shanks' extension, as explained in Van Dyke [11]. To the third order, these two methods are equivalent. However, for the surface vorticity, the improvement over the present third-order solution presented in Section 6.2 is insignificant. See Table I.

In our present work, we carry out the matched asymptotic solutions to the third-order by utilizing the Symbolic Manipulation Program due to Cole and Wolfram [4]. The surface quantities that compared well with the numerical solution of the full Navier–Stokes equations by Staniforth [10] are evaluated and plotted.

TABLE I

Comparison of First-, Second-, and Third-Order and Padé/Shank Improvement of Surface Vorticity for Aspect Ratio 0.6, Re = 2500, $\alpha = 0°$, $T = 0.5$

η	ω_1	ω_2	ω_3	Padé/Shank
0	0	0	0	0
10	17.9974	59.0541	44.3090	48.2052
20	33.1058	88.0573	75.9034	78.1046
30	44.2587	91.8030	87.2011	87.6073
40	51.9224	86.3535	85.8256	85.8335
50	57.0129	80.0950	80.8346	80.8591
60	60.3144	75.1075	76.0189	76.0788
70	62.3611	71.2440	72.0388	72.1169
80	63.4765	67.9057	68.5614	68.6754
90	63.8308	64.4868	65.0525	68.5927
100	63.4765	60.3833	60.9275	60.8461
110	62.3611	54.8870	55.4929	55.4474
120	60.3144	47.0544	47.8239	47.7817
130	57.0128	35.6376	36.6640	36.6170
140	51.9224	19.3981	20.5957	20.5532
150	44.2587	−1.2372	−0.6236	−0.6317
160	33.1058	−19.9188	−21.5575	−21.6098
170	17.9974	−21.8085	−25.3005	−25.6363
180	0	0	0	0

2. FORMULATION

The elliptic coordinates shown in Fig. 2 will be employed. See, for example, Milne-Thomson [8] or Yang [13]. Note the coordinates ξ, η, in Wang [12] are reversed in favor of more conventional notation. They are related to the rectangular Cartesian coordinates x, y by

$$\begin{aligned} x &= -c(\cosh\xi\cos\eta\cos\alpha - \sinh\xi\sin\eta\sin\alpha) \\ y &= c(\cosh\xi\cos\eta\sin\alpha + \sinh\xi\sin\eta\cos\alpha). \end{aligned} \tag{1}$$

Here α is the angle of attack and c is a constant to be determined having the dimension of length. Note also that the elliptic coordinate system is left-handed, so that when $\alpha = 0$, the front and rear stagnation points in the outer inviscid flow are at $\eta = 0$ and $\eta = \pi$, respectively; see Fig. 2. In general $\eta =$ constant yields confocal hyperbolas and $\xi =$ constant, confocal ellipses. The elliptic cylinder in question is represented by $\xi = \xi_o$. The metric in the plane is

$$\begin{aligned} (ds)^2 &= (dx)^2 + (dy)^2 \\ &= (h_1\,d\xi)^2 + (h_2\,d\eta)^2. \end{aligned}$$

From Eq. (1), one obtains

$$h = h_1 = h_2 = c(\cosh^2\xi - \cos^2\eta)^{1/2}. \tag{2}$$

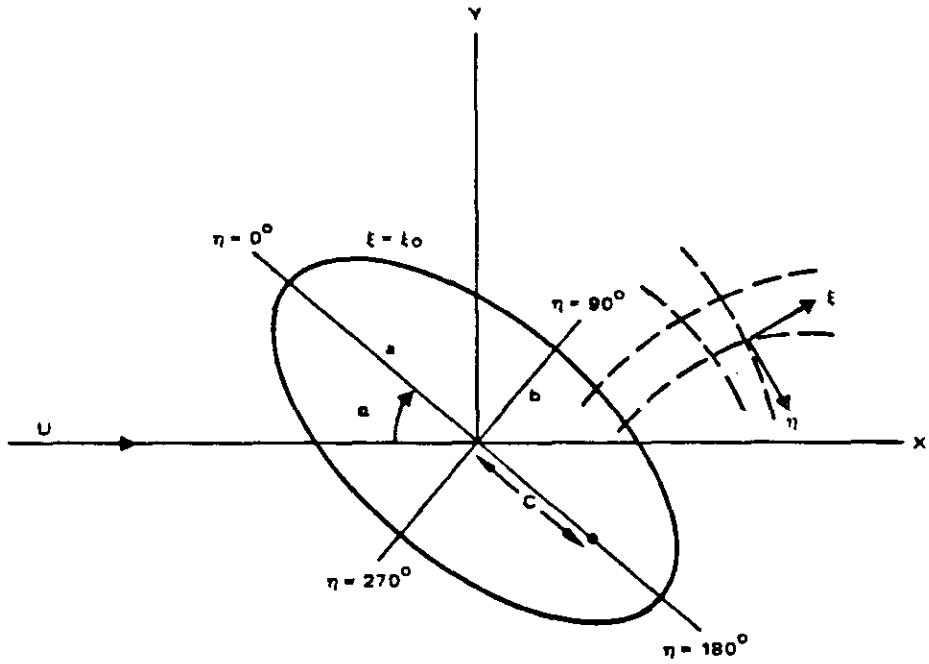

FIG. 2. Elliptic cylindrical coordinates.

The semi-major and semi-minor axes a and b of the ellipse are respectively

$$a = c \cosh \xi_o, \qquad b = c \sinh \xi_o. \tag{3}$$

The Navier–Stokes momentum equation for an incompressible fluid is

$$\frac{\partial \mathbf{u}}{\partial t} + \nabla\left(\frac{1}{2}u^2\right) - \mathbf{u} \times (\nabla \times \mathbf{u}) = -\frac{1}{\rho}\nabla p + \nu \nabla^2 \mathbf{u}. \tag{4}$$

Taking the curl, one obtains the vorticity equation

$$\frac{\partial \boldsymbol{\omega}}{\partial t} - \nabla \times (\mathbf{u} \times \boldsymbol{\omega}) = \nu \nabla^2 \boldsymbol{\omega}. \tag{5}$$

Here the vorticity $\boldsymbol{\omega}$ is the curl of the flow velocity $\mathbf{u}$ and ν is the kinematic viscosity coefficient of the fluid. Equation (5) is preferred to Eq. (4) in which the pressure is unknown. Thus we solve (5) for the vorticity and then the velocity field. The pressure field is to be determined from Eq. (4). When Eq. (5) is nondimensionalized by the characteristic length l, time T_0, and the impulsive flow velocity U, we obtain

$$\frac{\partial \boldsymbol{\omega}}{\partial t} - \frac{1}{\mathrm{St}} \nabla \times (\mathbf{u} \times \boldsymbol{\omega}) = \frac{1}{\mathrm{Re} \cdot \mathrm{St}} \nabla^2 \boldsymbol{\omega}, \tag{6}$$

where, as in Rosenhead [9],

$$\mathrm{Re} \equiv \frac{Ul}{\nu} = \text{Reynolds number} \tag{7}$$

$$\mathrm{St} \equiv \frac{l}{UT_0} = \text{Strouhal number} \tag{8}$$

and

$$l = \frac{1}{2}(a+b) = \frac{c}{2} e^{\xi_o}. \tag{9}$$

The case to be studied is the initial phase of the impulsively started viscous flow over an elliptic cylinder. To achieve a one-parameter type of expansion, ε, we assume, following Wang,

$$\varepsilon = \frac{1}{\mathrm{St}} = \frac{1}{\beta\,\mathrm{Re}} \ll 1, \tag{10}$$

where β is a constant of order one. Then

$$\varepsilon t = T \tag{11}$$

$$\varepsilon(\beta t)^{1/2} = \left(\frac{T}{\mathrm{Re}}\right)^{1/2}. \tag{12}$$

Equation (6) is now of the form

$$\frac{\partial \boldsymbol{\omega}}{\partial t} - \varepsilon \nabla \times (\mathbf{u} \times \boldsymbol{\omega}) = \beta \varepsilon^2 \nabla^2 \boldsymbol{\omega}. \tag{13}$$

The continuity equation

$$\nabla \cdot \mathbf{u} = 0 \tag{14}$$

is automatically satisfied by the introduction of the stream function $\psi(\xi, \eta)$ such that ξ- and η-velocity components are

$$u = -\frac{1}{h}\frac{\partial \psi}{\partial \eta} \tag{15}$$

$$v = \frac{1}{h}\frac{\partial \psi}{\partial \xi}, \tag{16}$$

where h is given by Eq. (2). For two-dimensional flow, the vorticity vector is

$$\boldsymbol{\omega} = (0, 0, \omega)$$

and

$$\omega = \nabla^2 \psi, \tag{17}$$

where

$$\nabla^2 = \frac{1}{h^2}\left(\frac{\partial^2}{\partial \xi^2} + \frac{\partial^2}{\partial \eta^2}\right). \tag{18}$$

Finally Eq. (13) becomes

$$\text{PDE,} \quad \left[\frac{\partial}{\partial t} + \frac{\varepsilon}{h^2}\left(\frac{\partial \psi}{\partial \xi}\frac{\partial}{\partial \eta} - \frac{\partial \psi}{\partial \eta}\frac{\partial}{\partial \xi}\right) - \varepsilon^2 \beta \nabla^2\right] \nabla^2 \psi = 0. \tag{19}$$

The initial and boundary conditions are

$$\text{IC,} \quad \psi(\xi, \eta, 0) = 2 \sinh(\xi - \xi_o) \sin(\eta + \alpha) \tag{20}$$

$$\text{BC,} \quad \psi(\xi_o, \eta, t) = \psi_\xi(\xi_o, \eta, t) = 0 \tag{21}$$

$$\psi(\xi, \eta, t) = 2 \sinh(\xi - \xi_o) \sin(\eta + \alpha) \quad \text{as} \quad \xi \to \infty. \tag{22}$$

Boundary condition (21) represents the familiar no-slip and vanishing normal velocity conditions at the surface of the ellipse. Initial condition (20) and the far-field boundary condition (22) both assert that the flow is potential, as given in Milne-Thomson [8].

3. MATCHED ASYMPTOTIC EXPANSIONS

The nonlinear system (19)–(22) is to be solved by the method of matched asymptotic expansions presented in Van Dyke [11] and Kevorkian and Cole [7]. The outer solution is expanded into

$$\psi^o(\xi, \eta, t; \varepsilon) = \psi_1^o(\xi, \eta, t) + \sum_{n=2} \delta_n(\varepsilon)\, \psi_n^o. \tag{23}$$

In the matching procedures, the gauge functions $\delta_n(\varepsilon)$'s are found to be

$$\delta_n(\varepsilon) = \varepsilon^{n-1}, \qquad n = 2, 3. \tag{24}$$

By substituting expansion (23) and (24) into Eq. (19) and applying initial condition (20), we obtain

$$\nabla^2 \psi_n^o = 0, \qquad n = 1, 2, 3. \tag{25}$$

With boundary condition (22), the first-order outer solution is

$$\psi_1^o(\xi, \eta, t) = 2 \sinh(\xi - \xi_o) \sin(\eta + \alpha). \tag{26}$$

In view of condition (22), the far-field boundary conditions for the remaining terms in expansion (23) is

$$\psi_n^o(\xi, \eta, t) = 0, \qquad \text{as} \quad \xi \to \infty, \qquad n = 2, 3. \tag{27}$$

The inner expansion for the stream function is

$$\psi^i(\xi, \eta, t; \varepsilon) = \sum_{n=1}^{3} \Delta_n(\varepsilon)\, \bar{\psi}_n^i(\bar{\xi}, \eta, t). \tag{28}$$

Again the gauge functions $\Delta_n(\varepsilon)$'s are found to be

$$\Delta_n(\varepsilon) = \varepsilon^n, \qquad n = 1, 2, 3. \tag{29}$$

The metric scale (2) is also expanded as

$$h(\xi, \eta) = h_1(\xi_o, \eta)[1 + \varepsilon \bar{\xi} h_2(\xi_o, \eta) + \varepsilon^2 \bar{\xi}^2 h_3(\xi_o, \eta) + \cdots], \tag{30}$$

where

$$\bar{\xi} = \frac{\xi - \xi_o}{\varepsilon} \tag{31}$$

$$h_1(\xi_o, \eta) = h(\xi_o, \eta)$$

$$h_2(\xi_o, \eta) = \frac{1}{h(\xi_o, \eta)}\frac{\partial h}{\partial \eta} \tag{32}$$

$$h_3(\xi_o, \eta) = \frac{1}{2h(\xi_o, \eta)}\frac{\partial^2 h}{\partial \eta^2}.$$

The outer and inner solutions are matched by applying the principle that the outer limit of the inner expansion is the same as the inner limit of the outer expansion. More explicitly, the m-term outer expansion of (the n-term inner expansion) equals the n-term inner expansion of (the m-term outer expansion). Matching conditions are thus developed; see Van Dyke [11].

4. ANALYTICAL SOLUTIONS

4.1. *First-Order Outer Expansion*

$$\text{PDE,}\quad \nabla^2\psi_1^o = 0 \tag{33}$$

$$\text{IC,}\quad \psi_1^o(\xi, \eta, 0) = 2\sinh(\xi - \xi_o)\sin(\eta + \alpha) \tag{34}$$

$$\text{BC,}\quad \psi_1^o(\xi, \eta, t) = 2\sinh(\xi - \xi_o)\sin(\eta + \alpha) \quad \text{as} \quad \xi \to \infty. \tag{35}$$

The solution is

$$\psi_1^o(\xi, \eta, t) = 2\sinh(\xi - \xi_o)\sin(\eta + \alpha). \tag{36}$$

The first-order outer solution is the potential flow solution as discussed in Milne-Thomson [8].

4.2. *First-Order Inner Expansion*

$$\text{PDE,}\quad \bar{\psi}^i_{1\bar{\xi}\bar{\xi}t} - \frac{\beta}{h_1^2}\bar{\psi}^i_{1\bar{\xi}\bar{\xi}\bar{\xi}\bar{\xi}} = 0 \tag{37}$$

$$\text{IC,}\quad \bar{\psi}^i_1(0, \eta, t) = 0 \quad \text{from (20)} \tag{38}$$

$$\text{BC,}\quad \bar{\psi}^i_1(0, \eta, t) = 0, \quad \bar{\psi}^i_{1\bar{\xi}}(0, \eta, t) = 0 \quad \text{from (21)} \tag{39}$$

$$\text{MC,}\quad \bar{\psi}^i_{1\bar{\xi}}(\infty, \eta, t) = \psi^o_{1\xi}(\xi_o, \eta, t) = 2\sin(\eta + \alpha) \quad \text{from (36).} \tag{40}$$

The solution is

$$\varepsilon\bar{\psi}^i_1(\zeta, \eta, t) = 4\left(\frac{T}{\mathrm{Re}}\right)^{1/2}\frac{1}{h_1(\eta)}\sin(\eta + \alpha) \times\left[\zeta(1 - \operatorname{erfc}\zeta) - \frac{1}{\pi^{1/2}}(1 - e^{-\zeta^2})\right], \tag{41}$$

where

$$\zeta = \frac{h_1(\eta)\,\bar{\xi}}{2(\beta t)^{1/2}}. \tag{42}$$

From Eqs. (30) and (32), one obtains

$$h_1(\eta) = 2e^{-\xi_o}(\sinh^2\xi_o + \sin^2\eta)^{1/2}. \tag{43}$$

Note the tangential velocity (16) is

$$v_1^i = \frac{1}{h_1}\bar{\psi}^i_{1\bar{\xi}}(\bar{\xi}, \eta, t) = \frac{1}{h_1(\eta)}2\sin(\eta + \alpha)[1 - \operatorname{erfc}\zeta]$$

which is comparable to the classical Rayleigh problem of an impulsively started flat plate.

4.3. *Second-Order Outer Expansion*

$$\text{PDE,}\quad \nabla^2\psi_2^o = 0 \tag{44}$$

$$\text{IC,}\quad \psi_2^o(\xi, \eta, 0) = 0 \tag{45}$$

$$\text{BC,}\quad \psi_2(\infty, \eta, t) = 0 \tag{46}$$

$$\text{MC,}\quad \psi_2^o(\xi_o, \eta, t) = \bar{\psi}^i_1(\infty, \eta, t) = -\frac{4}{\pi^{1/2}}\left(\frac{T}{\mathrm{Re}}\right)^{1/2} \times\frac{1}{h_1(\eta)}\sin(\eta + \alpha) \quad \text{from (41).} \tag{47}$$

The solution is

$$\varepsilon\psi_2^o(\xi, \eta, t) = -\frac{4e^{\xi_o}}{\pi^{3/2}}\left(\frac{T}{\mathrm{Re}}\right)^{1/2}\sum_{k=0}^{\infty}[\cos\alpha A'_k\sin k\eta + \sin\alpha B'_k\cos k\eta]\,e^{-k(\xi - \xi_o)} \tag{48}$$

in which

$$A'_k = \int_0^\pi \frac{\sin\eta\sin k\eta}{(\sinh^2\xi_o + \sin^2\eta)^{1/2}}\,d\eta$$

$$B'_k = \int_0^\pi \frac{\cos\eta\cos k\eta}{(\sinh^2\xi_o + \sin^2\eta)^{1/2}}\,d\eta.$$

4.4. *Second-Order Inner Expansion*

$$\text{PDE,}\quad \bar{\psi}^i_{2\bar{\xi}\bar{\xi}t} - \frac{\beta}{h_1^2}\bar{\psi}^i_{2\bar{\xi}\bar{\xi}\bar{\xi}\bar{\xi}} = \frac{1}{h_1^2}\bar{\psi}^i_{1\eta}\bar{\psi}^i_{1\bar{\xi}\bar{\xi}\bar{\xi}} - \frac{1}{h_1^2}\bar{\psi}^i_{1\bar{\xi}}\bar{\psi}^i_{1\bar{\xi}\bar{\xi}\eta} + \frac{2}{h_1^3}h_1'(\eta)\,\bar{\psi}^i_{1\bar{\xi}}\bar{\psi}^i_{1\bar{\xi}\bar{\xi}} - \frac{4\beta h_2}{h_1^2}\bar{\psi}^i_{1\bar{\xi}\bar{\xi}\bar{\xi}} - 2h_2\bar{\xi}\bar{\psi}^i_{1\bar{\xi}\bar{\xi}t} \tag{49}$$

$$\text{IC,}\quad \bar{\psi}^i_2(\bar{\xi}, \eta, 0) = 0 \tag{50}$$

$$\text{BC,}\quad \bar{\psi}^i_2(0, \eta, t) = 0 \tag{51}$$

$$\bar{\psi}^i_{2\bar{\xi}}(0, \eta, t) = 0 \tag{52}$$

$$\text{MC,}\quad \bar{\psi}^i_{2\bar{\xi}}(\infty, \eta, t) = \bar{\xi}\psi^o_{1\xi\xi}(\xi_o, \eta, t) + \psi^o_{2\xi}(\xi_o, \eta, t) = (\beta t)^{1/2}F(\eta) \tag{53}$$

in which from (48)

$$F(\eta) = \frac{4e^{\xi_o}}{\pi^{3/2}}\sum_{k=0}^{\infty}k(\cos\alpha A'_k\sin k\eta + \sin\alpha B'_k\cos k\eta).$$

The solution is

$$\varepsilon^2\bar{\psi}^i_2(\zeta,\eta,t) = -\frac{T}{\mathrm{Re}}\frac{h_2(\eta)}{h_1^2(\eta)}\sin(\eta+\alpha)\left[2\zeta^2\operatorname{erfc}\zeta-(1-\operatorname{erfc}\zeta)+\frac{2}{\pi^{1/2}}\zeta e^{-\zeta^2}\right]+2\frac{T}{\mathrm{Re}}\frac{1}{h_1(\eta)}F(\eta)\times\left[\frac{\pi^{1/2}}{2}\zeta^2\operatorname{erfc}\zeta-\frac{\pi^{1/2}}{4}(1-\operatorname{erfc}\zeta)+\frac{1}{2}\zeta(2-e^{-\zeta^2})\right]+8T\left(\frac{T}{\mathrm{Re}}\right)^{1/2}\frac{1}{h_1^3(\eta)}\sin(\eta+\alpha)\times\left[\cos(\eta+\alpha)-\frac{h_1'(\eta)}{h_1(\eta)}\sin(\eta+\alpha)\right]\times\left[-\frac{2}{3(\pi)^{1/2}}\zeta^2e^{-\zeta^2}\operatorname{erfc}\zeta-\frac{11}{6(\pi)^{1/2}}\times(1-e^{-\zeta^2}\operatorname{erfc}\zeta)+\frac{1}{3}\zeta^3\operatorname{erfc}^2\zeta-\frac{1}{2}\zeta\operatorname{erfc}^2\zeta-\left(1+\frac{4}{9\pi}\right)\zeta^3\operatorname{erfc}\zeta+\left(\frac{1}{2}-\frac{2}{3\pi}\right)\zeta\operatorname{erfc}\zeta-\frac{2}{3(\pi)^{1/2}}(1-\operatorname{erfc}\zeta)+\frac{8}{3(2\pi)^{1/2}}(1-\operatorname{erfc}2^{1/2}\zeta)+\frac{1}{3\pi}\zeta e^{-2\zeta^2}+\frac{1}{\pi^{1/2}}\left(1+\frac{4}{9\pi}\right)\zeta^2e^{-\zeta^2}-\frac{1}{\pi^{1/2}}\times\left(\frac{4}{9\pi}-\frac{3}{2}\right)(1-e^{-\zeta^2})\right]. \tag{54}$$

The above second-order solution agrees with that of Wang [12]. However, as previewed in Fig. 1, its numerical evaluation will be different from his.

4.5. *Third-Order Outer Solution*

$$\text{PDE,}\quad \nabla^2\psi_3^o=0 \tag{55}$$

$$\text{IC,}\quad \psi_3^o(\xi,\eta,0)=0 \tag{56}$$

$$\text{BC,}\quad \psi_3^o(\infty,\eta,t)=0 \tag{57}$$

$$\text{MC,}\quad \psi_3^o(\xi_o,\eta,t)=\bar{\psi}^i_2(\infty,\eta,t)=\beta t\frac{h_2(\eta)}{h_1^2(\eta)}\sin(\eta+\alpha)-\frac{\beta t(\pi)^{1/2}}{2h_1(\eta)}F(\eta)+\frac{8}{(\pi)^{1/2}}\times\left(\frac{8}{3(2)^{1/2}}-\frac{4}{9\pi}-1\right)\frac{t(\beta t)^{1/2}}{h_1(\eta)}\times\left[\frac{1}{h_1^2(\eta)}\sin(\eta+\alpha)\cos(\eta+\alpha)-\frac{h_1'(\eta)}{h_1^3(\eta)}\times\sin^2(\eta+\alpha)\right]\quad\text{from (54).} \tag{58}$$

The solution is

$$\varepsilon^2\psi_3^o(\xi,\eta,t)=\frac{T}{\mathrm{Re}}\left\{\frac{e^{2\xi_o}\sinh 2\xi_o}{4\pi}\sum_{k=0}^{\infty}(\cos\alpha A_k''\sin k\eta+\sin\alpha B_k''\cos k\eta)\,e^{-k(\xi-\xi_o)}-\frac{2e^{2\xi_o}}{\pi^2}\times\sum_{k=0}^{\infty}\left[\cos\alpha\left(\sum_{j=0}^{\infty}jA_j'A_{j,k}^{\mathrm{vi}}\right)\sin k\eta+\sin\alpha\left(\sum_{j=0}^{\infty}jB_j'B_{j,k}^{\mathrm{vi}}\right)\cos k\eta\right]e^{-k(\xi-\xi_o)}\right\}+\frac{e^{3\xi_o}}{\pi^{3/2}}\left(\frac{8}{3(2)^{1/2}}-\frac{4}{9\pi}-1\right)T\left(\frac{T}{\mathrm{Re}}\right)^{1/2}\times\left\{\sum_{k=1}^{\infty}\left[\left(\cos2\alpha A_k'''-\frac{1}{2}A_k^{\mathrm{iv}}+\frac{1}{4}\cos2\alpha A_k^{\mathrm{v}}\right)\sin2k\eta+\left(\sin2\alpha B_k''-\frac{1}{2}\sin2\alpha B_k^{\mathrm{iv}}\right)\cos2k\eta d\,e^{-2k(\xi-\xi_o)}+\frac{1}{2}\left(\sin2\alpha B_o''-\frac{1}{2}\sin2\alpha B_o^{\mathrm{iv}}\right)\right\} \tag{59}$$

in which

$$A_k''=\int_0^{\pi}\frac{\sin\eta\sin k\eta}{(\sinh^2\xi_o+\sin^2\eta)^2}\,d\eta,$$

$$A_{j,k}^{\mathrm{vi}}=\int_0^{\pi}\frac{\sin j\eta\sin k\eta}{(\sinh^2\xi_o+\sin^2\eta)^{1/2}}\,d\eta,$$

$$A_k'''=\int_0^{\pi}\frac{\sin2\eta\sin2k\eta}{(\sinh^2\xi_o+\sin^2\eta)^{3/2}}\,d\eta,$$

$$A_k^{\mathrm{iv}}=\int_0^{\pi}\frac{\sin2\eta\sin2k\eta}{(\sinh^2\xi_o+\sin^2\eta)^{5/2}}\,d\eta,$$

$$A_k^{\mathrm{v}}=\int_0^{\pi}\frac{\sin4\eta\sin2k\eta}{(\sinh^2\xi_o+\sin^2\eta)^{5/2}}\,d\eta,$$

$$B_k''=\int_0^{\pi}\frac{\cos\eta\cos k\eta}{(\sinh^2\xi_o+\sin^2\eta)^2}\,d\eta$$

$$B_{j,k}^{\mathrm{vi}}=\int_0^{\pi}\frac{\cos j\eta\cos k\eta}{(\sinh^2\xi_o+\sin^2\eta)^{1/2}}\,d\eta$$

$$B_k'''=\int_0^{\pi}\frac{\cos2\eta\cos2k\eta}{(\sinh^2\xi_o+\sin^2\eta)^{3/2}}\,d\eta$$

$$B_k^{\mathrm{iv}}=\int_0^{\pi}\frac{\sin^2 2\eta\cos2k\eta}{(\sinh^2\xi_o+\sin^2\eta)^{5/2}}\,d\eta.$$

4.6. *Third-Order Inner Expansion*

$$\text{PDE,}\quad \bar\psi^{i}_{3\bar\xi\bar\xi t}-\frac{\beta}{h_1^2}\bar\psi^{i}_{3\bar\xi\bar\xi\bar\xi\bar\xi}=\frac{1}{h_1^2}\bar\psi^{i}_{1\eta}\bar\psi^{i}_{2\bar\xi\bar\xi\bar\xi}$$
$$-\frac{1}{h_1^2}\bar\psi^{i}_{1\bar\xi}\bar\psi^{i}_{2\bar\xi\bar\xi\eta}+\frac{2h_1'}{h_1^3}\bar\psi^{i}_{1\bar\xi}\bar\psi^{i}_{2\bar\xi\bar\xi}$$
$$+\frac{1}{h_1^2}\bar\psi^{i}_{1\bar\xi\bar\xi\bar\xi}\bar\psi^{i}_{2\eta}-\frac{1}{h_1^2}\bar\psi^{i}_{1\bar\xi\bar\xi\eta}\bar\psi_{2\bar\xi}$$
$$+\frac{2h_1'}{h_1^3}\bar\psi^{i}_{1\bar\xi\bar\xi}\bar\psi^{i}_{2\bar\xi}-\frac{2h_2}{h_1^2}\bar\xi\bar\psi^{i}_{1\eta}\bar\psi^{i}_{1\bar\xi\bar\xi\bar\xi}$$
$$+\frac{2h_2}{h_1^2}\bar\xi\bar\psi^{i}_{1\bar\xi}\bar\psi^{i}_{1\bar\xi\bar\xi\eta}$$
$$+2\bar\xi\left(\frac{h_2'}{h_1^2}-\frac{2h_2h_1'}{h_1^3}\right)$$
$$\times\bar\psi^{i}_{1\bar\xi}\bar\psi^{i}_{1\bar\xi\bar\xi}-\frac{2h_2}{h_1^2}\bar\psi^{i}_{1\eta}\bar\psi^{i}_{1\bar\xi\bar\xi}$$
$$-\bar\psi^{i}_{\eta\eta t}+\beta\left[\frac{3h_2^2-2h_3}{h_1^2}\bar\xi^2\bar\psi^{i}_{1\bar\xi\bar\xi\bar\xi\bar\xi}\right.$$
$$+\frac{2}{h_1^2}\bar\psi^{i}_{1\bar\xi\bar\xi\eta\eta}+\frac{4}{h_1^2}(3h_2^2-2h_3)\bar\xi\bar\psi^{i}_{1\bar\xi\bar\xi\bar\xi}$$
$$-\frac{4h_1'}{h_1^3}\bar\psi^{i}_{1\bar\xi\bar\xi\eta}+\frac{2}{h_1^2}\left(3h_2^2-2h_3+\frac{3h_1'^2}{h_1^2}-\frac{h_1''}{h_1}\right)\bar\psi^{i}_{1\bar\xi\bar\xi}$$
$$\left.-\frac{2h_2}{h_1^2}\bar\xi\bar\psi^{i}_{2\bar\xi\bar\xi\bar\xi\bar\xi}-\frac{4h_2}{h_1^2}\bar\psi^{i}_{2\bar\xi\bar\xi\bar\xi}\right] \tag{60}$$

$$\text{IC,}\quad \bar\psi^{i}_{3}(\bar\xi,\eta,0)=0 \tag{61}$$

$$\text{BC,}\quad \bar\psi^{i}_{3}(0,\eta,t)=0,\qquad \bar\psi^{i}_{3\bar\xi}(0,\eta,t)=0 \tag{62}$$

$$\text{MC,}\quad \bar\psi^{i}_{3\bar\xi}(\infty,\eta,t)=\frac{\bar\xi^2}{2}\psi^{o}_{1\xi\xi\xi}(\xi_o,\eta)+\bar\xi\psi^{o}_{2\xi\xi}(\xi_o,\eta,t)$$
$$+\psi^{o}_{3\xi}(\xi_o,\eta,t)=\bar\xi^2\sin(\eta+\alpha)$$
$$-(\beta t)^{1/2}\bar\xi G_1(\eta)-\beta tG_2(\eta)+\beta tG_4(\eta)$$
$$-t(\beta t)^{1/2}G_3(\eta)\qquad\text{from (59)} \tag{63}$$

in which

$$G_1(\eta)=\frac{4e^{\xi_o}}{\pi^{3/2}}\sum_{k=0}^{\infty}k^2[\cos\alpha A_k'\sin k\eta+\sin\alpha B_k'\cos k\eta]$$

$$G_2(\eta)=\frac{e^{2\xi_o}\sinh 2\xi_o}{4\pi}\sum_{k=1}^{\infty}k[\cos\alpha A_k''\sin k\eta+\sin\alpha B_k''\cos k\eta]$$

$$G_3(\eta)=\frac{3}{2}\frac{e^{3\xi_o}}{\pi^{3/2}}\left(\frac{8}{3(2)^{1/2}}-\frac{4}{9\pi}-1\right)\times\sum_{k=1}^{\infty}k\left[\left(\cos 2\alpha A_k'''-\frac{1}{2}A_k^{\mathrm{iv}}+\frac{1}{4}\cos 2\alpha A_k^{\mathrm{v}}\right)\sin 2k\eta+\left(\sin 2\alpha B_k'''-\frac{1}{2}\sin 2\alpha B_k^{\mathrm{iv}}\right)\cos 2k\eta\right]$$

$$G_4(\eta)=\frac{2e^{2\xi_o}}{\pi^2}\sum_{k=1}^{\infty}k\left[\cos\alpha\left(\sum_{j=1}^{\infty}jA_j'A_{j,k}^{\mathrm{vi}}\right)\sin k\eta+\sin\alpha\left(\sum_{j=1}^{\infty}jB_j'B_{j,k}^{\mathrm{vi}}\right)\cos k\eta\right].$$

The solution is

$$\varepsilon^2\bar\psi^{i}_{3\bar\xi}(\zeta,\eta,t)$$
$$=-2\frac{T}{\mathrm{Re}}\frac{1}{h_1^2}\sin(\eta+\alpha)K_0(\zeta)+\frac{T}{\mathrm{Re}}\frac{1}{h_1}G_1(\eta)K_1(\zeta)$$
$$+\frac{T}{\mathrm{Re}}[G_4(\eta)-G_2(\eta)]K_2(\zeta)$$
$$-\frac{T}{\mathrm{Re}}\frac{h_1'^2}{h_1^4}\sin(\eta+\alpha)J_1(\zeta)$$
$$-\frac{T}{\mathrm{Re}}\frac{h_1''}{h_1^3}\sin(\eta+\alpha)J_2(\zeta)-\frac{T}{\mathrm{Re}}\frac{h_2^2}{h_1^2}\sin(\eta+\alpha)J_3(\zeta)$$
$$-\frac{T}{\mathrm{Re}}\frac{h_3}{h_1^2}\sin(\eta+\alpha)J_4(\zeta)-\frac{T}{\mathrm{Re}}\frac{1}{h_1^2}\sin(\eta+\alpha)J_5(\zeta)$$
$$-\frac{T}{\mathrm{Re}}\frac{h_1'}{h_1^3}\cos(\eta+\alpha)J_6(\zeta)-\frac{T}{\mathrm{Re}}\frac{h_2}{h_1}F(\eta)J_7(\zeta)$$
$$-\frac{3}{2}T\left(\frac{T}{\mathrm{Re}}\right)^{1/2}G_3(\eta)K_3(\zeta)$$
$$-T\left(\frac{T}{\mathrm{Re}}\right)^{1/2}\frac{h_1'h_2}{h_1^4}\sin^2(\eta+\alpha)J_8(\zeta)$$
$$-T\left(\frac{T}{\mathrm{Re}}\right)^{1/2}\frac{h_2}{h_1^3}\sin(\eta+\alpha)\cos(\eta+\alpha)J_9(\zeta)$$
$$-T\left(\frac{T}{\mathrm{Re}}\right)^{1/2}\frac{F(\eta)}{h_1^2}\cos(\eta+\alpha)J_{10}(\zeta)$$
$$-T\left(\frac{T}{\mathrm{Re}}\right)^{1/2}\frac{F(\eta)h_1'}{h_1^3}\sin(\eta+\alpha)J_{11}(\zeta)$$
$$-T\left(\frac{T}{\mathrm{Re}}\right)^{1/2}\frac{h_2'}{h_1^3}\sin^2(\eta+\alpha)J_{12}(\zeta)$$
$$-T\left(\frac{T}{\mathrm{Re}}\right)^{1/2}\frac{F'(\eta)}{h_1^2}\sin(\eta+\alpha)J_{13}(\zeta)$$
$$-T^2\frac{h_1'^2}{h_1^6}\sin^3(\eta+\alpha)J_{14}(\zeta)$$
$$-T^2\frac{1}{h_1^4}\sin(\eta+\alpha)J_{15}(\zeta)-T^2\frac{1}{h_1^4}\sin^3(\eta+\alpha)J_{16}(\zeta)$$
$$-T^2\frac{h_1''}{h_1^5}\sin^3(\eta+\alpha)J_{17}(\zeta)-T^2\frac{h_1'}{h_1^5}\cos(\eta+\alpha)J_{18}(\zeta)$$
$$-T^2\frac{h_1'}{h_1^5}\cos^3(\eta+\alpha)J_{19}(\zeta) \tag{64}$$

in which

$$K_0(\zeta) = -2\zeta^2$$

$$K_1(\zeta) = 2\zeta$$

$$K_2(\zeta) = -\left[(1+2\zeta^2)\operatorname{erfc}\zeta - \frac{2}{\pi^{1/2}}\zeta e^{-\zeta^2}\right] + 1$$

$$K_3(\zeta) = -\frac{\pi^{1/2}}{3}\left[-(3\zeta+2\zeta^3)\operatorname{erfc}\zeta + (1+\zeta^2)\frac{2}{\pi^{1/2}}e^{-\zeta^2}\right] + \frac{2}{3}$$

$$\begin{aligned} J_1(\zeta) = {} & \left[16\pi^{1/2}I_5(\infty) + 8\pi^{1/2}I_{11}(\infty) - \frac{7}{2}\right] \\ & \times \left[(1+2\zeta^2)(1-\operatorname{erfc}\zeta) + \frac{2}{\pi^{1/2}}\zeta e^{-\zeta^2}\right] \\ & + \frac{7}{2}(1+2\zeta^2) - \frac{7}{\pi^{1/2}}\zeta e^{-\zeta^2} - \frac{40}{3\pi^{1/2}}\zeta^3 e^{-\zeta^2} \\ & - \frac{7}{2}\operatorname{erfc}\zeta + \zeta^2\operatorname{erfc}\zeta + 16\zeta^4\operatorname{erfc}\zeta \\ & + 8\pi^{1/2}\operatorname{erfc}\zeta(1+2\zeta^2)[2I_2(\zeta) + I_{14}(\zeta)] \\ & - 8\pi^{1/2}(1+2\zeta^2)[2I_5(\zeta) + I_{11}(\zeta)], \end{aligned}$$

where

$$I_2(\zeta) = \int_0^\zeta \zeta^2 e^{\zeta^2}\operatorname{erfc}\zeta\, d\zeta$$

$$I_5(\zeta) = \int_0^\zeta \zeta^2 e^{\zeta^2}\operatorname{erfc}^2\zeta\, d\zeta$$

$$I_{11}(\zeta) = \int_0^\zeta e^{\zeta^2}\operatorname{erfc}^2\zeta\, d\zeta$$

$$I_{14}(\zeta) = \int_0^\zeta e^{\zeta^2}\operatorname{erfc}\zeta\, d\zeta.$$

The remaining $J(\zeta)$'s are lengthy expressions, which will not be reproduced here. Similar expressions may be found in Hermel [6]. The third-order solutions presented here are new and important for the reasons given in the Introduction.

5. SURFACE QUANTITIES

The surface quantities are obtained from the inner solution to the third order.

5.1. *Vorticity*

$$\begin{aligned} \omega(\xi_o, \eta, t) = {} & \frac{1}{2h(\xi_o, \eta)}\left(\frac{\mathrm{Re}}{T}\right)^{1/2}[\bar{\psi}^{i}_{1\bar{\xi}\zeta}(0,\eta,t) + \varepsilon\bar{\psi}^{i}_{2\bar{\xi}\zeta}(0,\eta,t) \\ & + \varepsilon^2\bar{\psi}^{i}_{3\bar{\xi}\zeta}(0,\eta,t) + O(\varepsilon^3)], \end{aligned} \tag{65}$$

recalling Eqs. (41), (54), and (64).

5.2. *Progression of Separation Point with Time*

This is solved from the condition for flow separation

$$\omega(\xi_o, \eta, t) = 0,$$

or from

$$\bar{\psi}^{i}_{1\bar{\xi}\zeta}(0,\eta,t) + \varepsilon\bar{\psi}^{i}_{2\bar{\xi}\zeta}(0,\eta,t) + \varepsilon^2\bar{\psi}^{i}_{3\bar{\xi}\zeta}(0,\eta,t) = 0. \tag{66}$$

5.3. *Pressure Coefficient*

The pressure distribution on the elliptic cylinder is expressed in terms of the pressure coefficient defined as

$$C_p \equiv \frac{p(\xi_o,\eta,t) - p_\infty}{\rho U^2/2} = C_{p_1} + C_{p_2} \tag{67}$$

in which p_∞ is the free-stream pressure. For expediency, we evaluate the first term

$$\begin{aligned} C_{p_1}(\xi_o,\eta,t) \equiv {} & \frac{p(\xi_o,\eta,t) - p(\xi_o,\alpha,t)}{\rho U^2/2} \\ = {} & \frac{2}{\mathrm{Re}}\int_0^\eta \left(\frac{\partial\omega}{\partial\xi}\right)_{\xi_o} d\eta \\ = {} & \frac{1}{2T}\int_0^\eta [\bar{\psi}^{i}_{1\bar{\xi}\zeta\zeta}(0,\eta,t) + \varepsilon\bar{\psi}^{i}_{2\bar{\xi}\zeta\zeta}(0,\eta,t) \\ & + \varepsilon^2\bar{\psi}^{i}_{3\bar{\xi}\zeta\zeta}(0,\eta,t)]\, d\eta - \frac{2}{(T\cdot\mathrm{Re})^{1/2}} \\ & \times \int_0^\eta \frac{h_2(\xi_o,\eta)}{h_1(\xi_o,\eta)}[\bar{\psi}^{i}_{1\bar{\xi}\zeta}(0,\eta,t) + \varepsilon\bar{\psi}^{i}_{2\bar{\xi}\zeta}(0,\eta,t) \\ & + \varepsilon^2\bar{\psi}^{i}_{3\bar{\xi}\zeta}(0,\eta,t)]\, d\eta. \end{aligned} \tag{68}$$

The second term is one, which may be obtained from the potential flow solution in Milne-Thomson [8, p. 171] with $\eta = \alpha$:

$$\begin{aligned} C_{p_2}(\xi_o,\eta,t) \equiv {} & \frac{p(\xi_o,\eta,t) - p_\infty}{\rho U^2/2} \\ = {} & 1 - \left(\frac{1+b/a}{1-b/a}\right)\frac{1-\cos 2(\eta-\alpha)}{\cosh 2\xi_o - \cos 2\eta}. \end{aligned} \tag{69}$$

5.4. *Drag Coefficient*

The drag consists of the pressure and friction parts:

$$C_D = C_{D_p} + C_{D_f} \tag{70}$$

$$\begin{aligned} C_{D_p} = {} & \frac{4e^{-\xi_o}}{\mathrm{Re}}\left[+\cosh\xi_0\sin\alpha\int_0^{2\pi}\left(\frac{\partial\omega}{\partial\xi}\right)_{\xi_o}(1-\cos\eta)\, d\eta \right. \\ & \left. - \sinh\xi_o\cos\alpha\int_0^{2\pi}\left(\frac{\partial\omega}{\partial\xi}\right)_{\xi_o}\sin\eta\, d\eta\right] \end{aligned} \tag{71}$$

$$C_{D_f}=\frac{4e^{-\xi_o}}{\mathrm{Re}}\left[\cosh\xi_0\cos\alpha\int_0^{2\pi}(\omega)_{\xi_o}\sin\eta\,d\eta\right.$$
$$\left.+\sinh\xi_o\sin\alpha\int_0^{2\pi}(\omega)_{\xi_o}\cos\eta\,d\eta\right]. \tag{72}$$

5.5. *Lift Coefficient*

Similarly the lift coefficient is

$$C_L=C_{L_p}+C_{L_f} \tag{73}$$
$$C_{L_p}=\frac{4e^{-\xi_o}}{\mathrm{Re}}\left[+\cosh\xi_0\cos\alpha\int_0^{2\pi}\left(\frac{\partial\omega}{\partial\xi}\right)_{\xi_o}(1-\cos\eta)\,d\eta\right.$$
$$\left.+\sinh\xi_o\sin\alpha\int_0^{2\pi}\left(\frac{\partial\omega}{\partial\xi}\right)_{\xi_o}\sin\eta\,d\eta\right] \tag{74}$$
$$C_{L_f}=\frac{4e^{-\xi_o}}{\mathrm{Re}}\left[-\cosh\xi_0\sin\alpha\int_0^{2\pi}(\omega)_{\xi_o}\sin\eta\,d\eta\right.$$
$$\left.+\sinh\xi_o\cos\alpha\int_0^{2\pi}(\omega)_{\xi_o}\cos\eta\,d\eta\right]. \tag{75}$$

6. RESULTS

The analytical solutions to the third order obtained for an impulsively started incompressible, viscous flow over an elliptic cylinder have been evaluated numerically. To compare with the numerical solutions of Staniforth [10], we consider an elliptic cylinder with aspect ratio

$$\frac{b}{a}=0.6, \qquad \text{i.e.,} \quad \xi_o=0.6931471805$$

at Re = 2500. Note that the Reynolds number defined in our present work is half of that defined by Staniforth. The case of the infinite Reynolds number corresponding to the boundary layer rather than the fully viscous flow is also investigated. Several angles of attack were considered in the computation.

6.1. *Flow Pattern*

The second-order inner solution of the stream-function (54) which contributes to the third-order composite solution is plotted in Fig. 3 for aspect ratio 0.6, Re = 2500, $T=1.0$, and $\alpha=0°$, 45°, and 90°. Figure 3a shows the symmetric flow pattern with the magnified bubble in Fig. 3b. For $T=0.5$, the bubble is not quite discernible. So, we plot the flow contour for $T=1.0$, where we stretched to the limit of the theory. Figures 3c and d are for $\alpha=45°$, for which the flow is no longer symmetric. Figures 3e and f show the flow contour at $\alpha=90°$ which is again symmetric along the flow direction. Figures 3 should be viewed together with Figs. 4 to observe the separation and reattachment of the flow.

6.2. *Vorticity*

The vorticity on the surface of the elliptic cylinder as given by Eq. (65) for Re = 2500 is evaluated and plotted in Figs. 4a, b, and c. Figure 4a is for angle of attack $\alpha=0$. The flow for this case is symmetric. For nondimensional time $T\leqslant 0.2$, the flow is attached. At $T=0.35$, the flow separated at $T=0.25$ (Fig. 7) at the rear stagnation point and the separation bubble grows with time. At $T=0.5$, the bubble spans from $\eta\simeq 150°$ to the rear stagnation point $\eta=180°$. As mentioned in the Introduction, the Padé approximant and Shank extension to the third order are the same. For example, the improved surface vorticity, $\omega_{p/s}$, is given in terms of the first-, second-, and third-order vorticity as

$$\omega_{p/s}=\frac{\omega_3\omega_1-\omega_2^2}{\omega_3+\omega_1-2\omega_2}.$$

These values are tabulated in Table I for the ellipse of aspect ratio 0.6, Reynolds number 2500, zero angle of attack, and time 0.5. We see that the first-order solution, being symmetric does not predict flow separation. The second, third, and Padé–Shank solutions show the flow separation bubble. The second-order solution is improved by the third. However, the third-order solution and Padé–Shank improvement are in good agreement. Figure 4b is for $\alpha=45°$, where the flow is no longer symmetric. For $T\leqslant 0.2$, the flow is attached. For $T\geqslant 0.35$, however, the flow is already separated, the bubble growing from the rear stagnation point $\eta=135°$ to about $\eta=182°$. It is to be noted that the flow rotation is counterclockwise between $\eta=135°$ and 315° and is consequently shown to be negative in Fig. 4b. Figure 4c shows the surface vorticity for $\alpha=90°$. Again the flow is symmetric. In fact, we could consider this case, an elliptic cylinder with aspect ratio $b/a=0.6$ at an angle of attack $\alpha=90°$, equivalently as an elliptic cylinder with $b/a=1/0.6=1.6$ at $\alpha=0°$. Therefore, the surface vorticity distribution between $\eta=90°$ and 270° is a mirror image of the surface vorticity between $\eta=270°$ and $\eta=90°$ in Fig. 4c. For $T\leqslant 0.2$, the flow is attached. For $T\geqslant 0.35$, the flow is separated. The bubbles are growing from $\eta\simeq 132°$ to 162° and symmetrically from $\eta\simeq 48°$ to 18°. Figures 4a, b, and c compare very favorably with Figs. 11, 14, and 15 of Staniforth [10].

For Re = ∞, the corresponding figures look qualitatively the same as Figs. 4a, b, and c, respectively. They do not agree as favorably, however, with Figs. 3, 6, and 7 of Staniforth [10] whose results are based on boundary layer formulations.

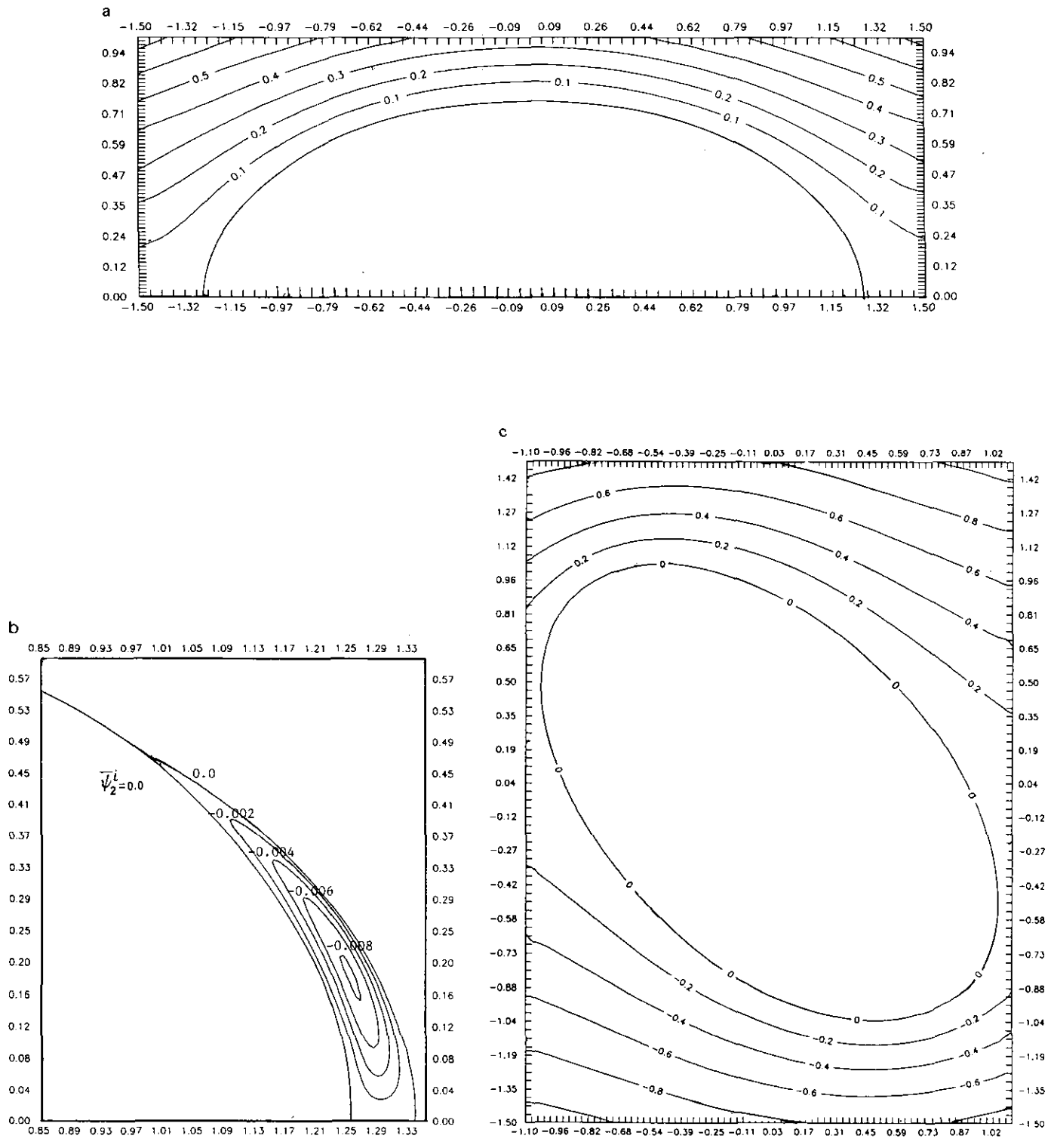

FIG. 3. Flow pattern for aspect ratio 0.6, Re = 2500, $T = 1.0$: (a) $\alpha = 0°$; (b) magnified view of the separation bubble at $\alpha = 0°$; (c) $\alpha = 45°$; (d) magnified view of the separation bubble at $\alpha = 45°$; (e) $\alpha = 90°$; (f) magnified view of the separation bubble at $\alpha = 90°$.

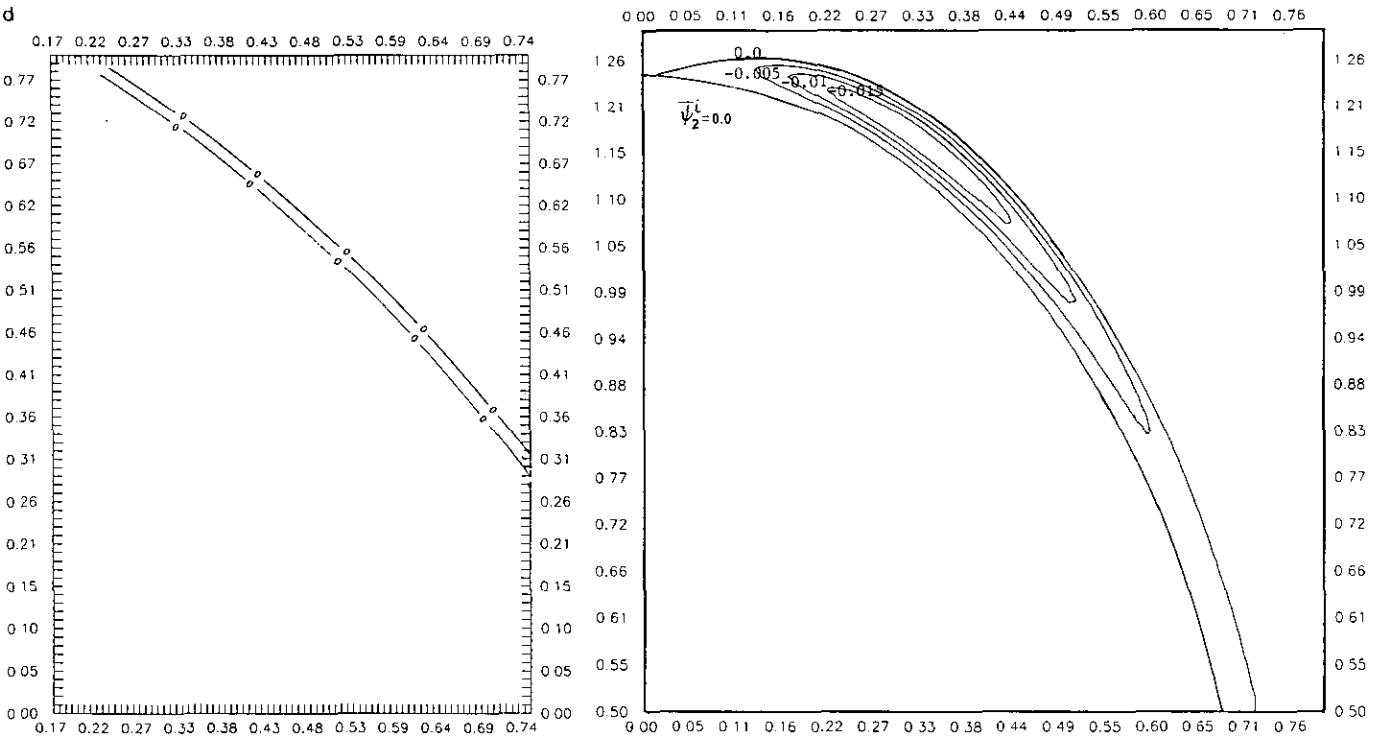

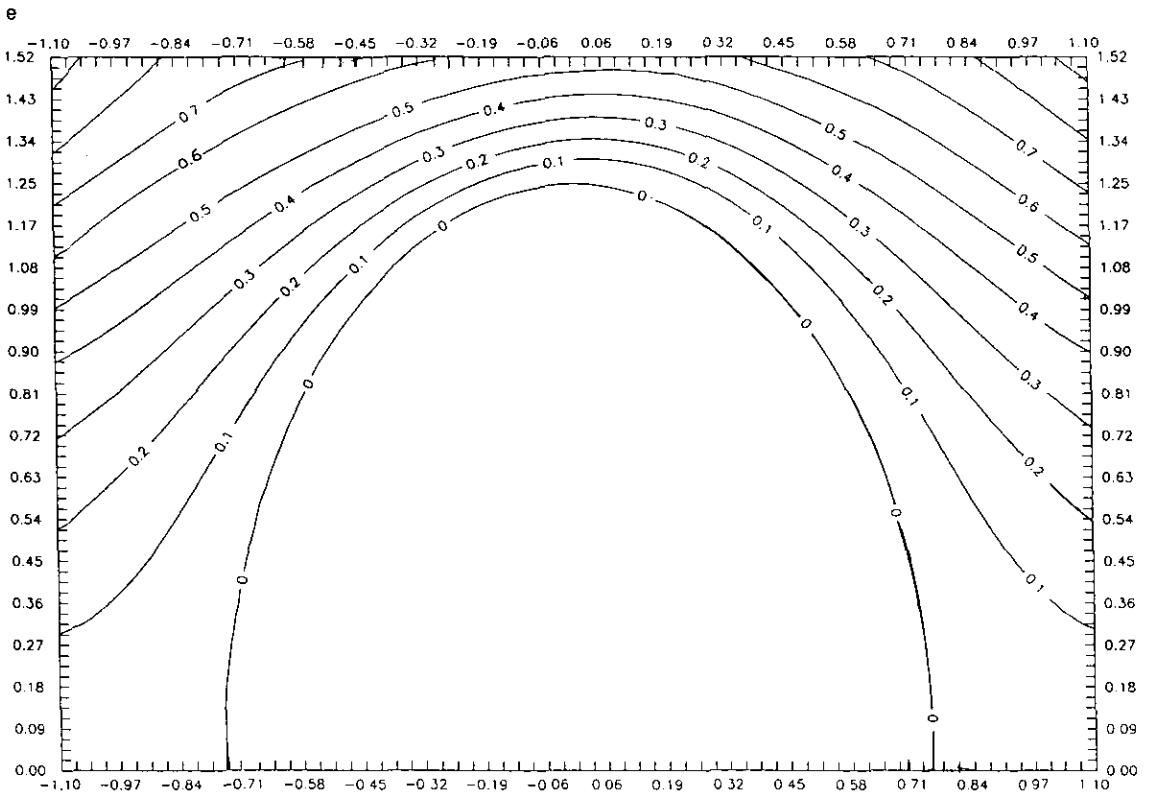

FIG. 3—*Continued*

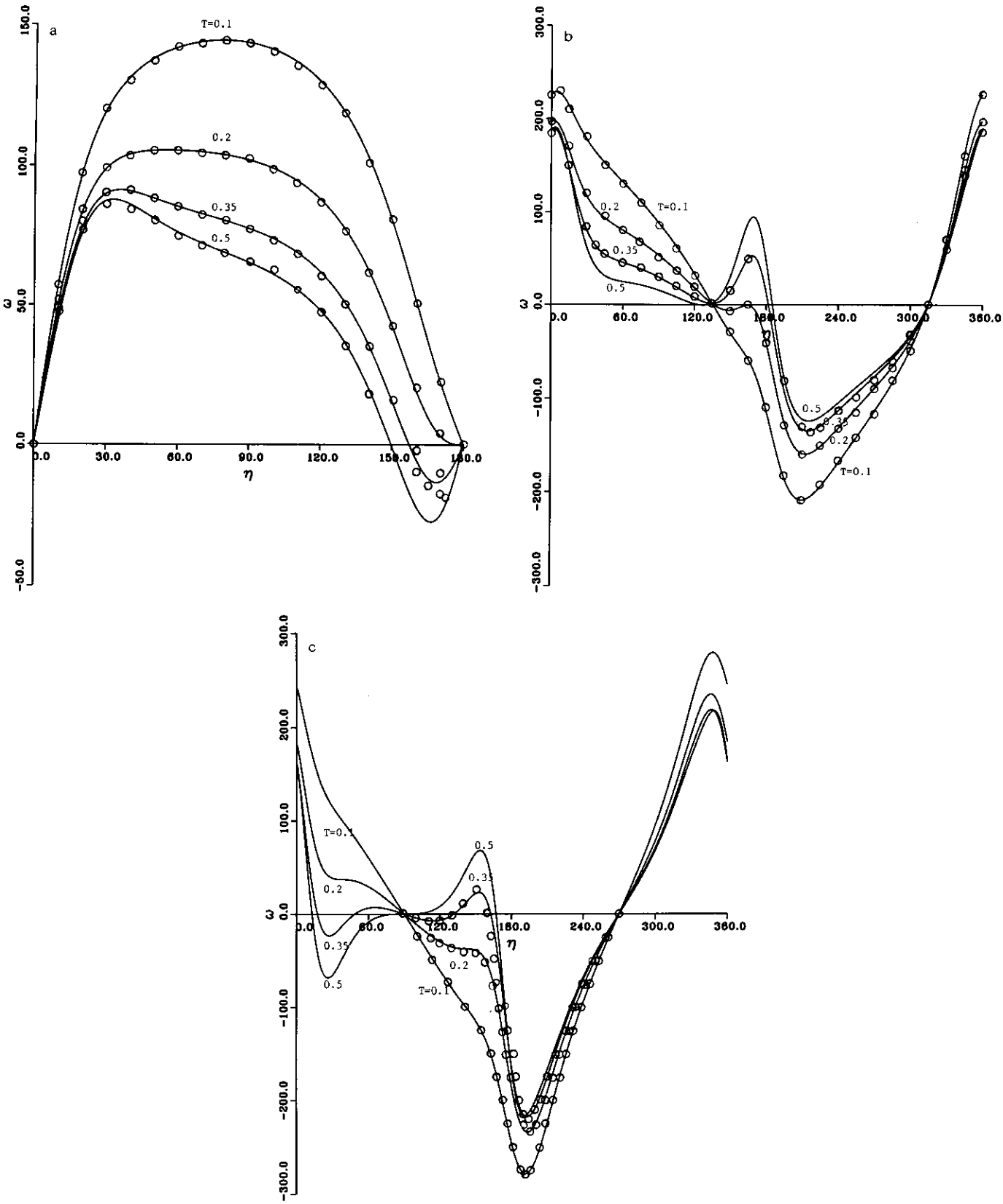

FIG. 4. Development of the surface vorticity for an elliptic cylinder with aspect ratio 0.6, Re = 2500; ○, Staniforth [10]: (a) $\alpha = 0°$; (b) $\alpha = 45°$; (c) $\alpha = 90°$.

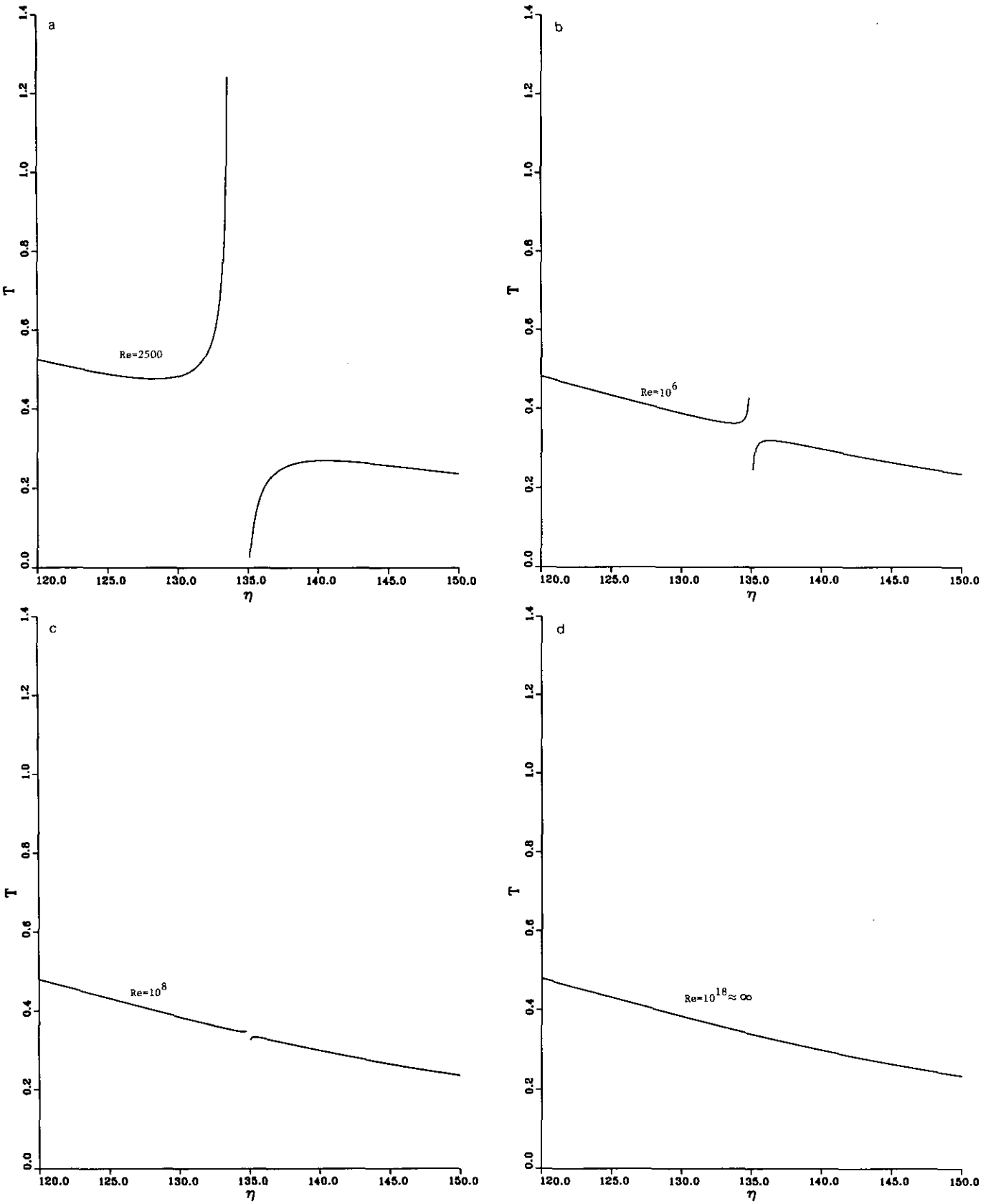

FIG. 5. Movement of the separation and reattachment points in the vicinity of discontinuity for an elliptic cylinder with aspect ratio 0.6, and $\alpha = 45°$: (a) $\mathrm{Re} = 2500$; (b) $\mathrm{Re} = 10^6$; (c) $\mathrm{Re} = 10^8$; (d) $\mathrm{Re} = 10^{18} \approx \infty$.

6.3. *Progression of Separation with Time*

The time progression of the separation points, where velocity and shear simultaneously vanish, given by Eq. (66), for a $b/a = 0.6$ ellipse at $\alpha = 45°$, $\mathrm{Re} = 2500$, looks qualitatively like Fig. 1. A discontinuity occurs at $\eta = \pi - \alpha = 135°$. As shown in Fig. 5 the severity of this discontinuity diminishes as the Reynolds number increases. Recall that the asymptotic solution is valid for small time and large Reynolds number. At $\mathrm{Re} = 2500$, the gap between the two curves is $\Delta T \approx 0.2$. At $\mathrm{Re} = 10^6$, $\Delta T \approx 0.04$; $\mathrm{Re} = 10^8$, $\Delta T \approx 0.01$, and at $\mathrm{Re} = 10^{18} \approx \infty$, the discontinuity essentially vanishes. Strictly speaking, the present solution is valid for Reynolds numbers over 10^6. But comparing with the numerical computation of Staniforth, the other quantities obtained for $\mathrm{Re} = 2500$ in the present work are quite acceptable. Incidently, his work does not show any discontinuity.

The progression of the separation points for flow past an elliptic cylinder with aspect ratio 0.6, Reynolds number $10^9 \approx \infty$, and angles of attack $\alpha = 0°$, 45°, and 90° are plotted in Fig. 6. At $\alpha = 0$, the flow starts to separate at the rear stagnation point $\eta = 180°$ at $T = 0.19$. The symmetric separation bubble then grows gradually with time. At $\alpha = 90°$, the flow is again symmetric, but starts to separate at two locations $\eta = 29°$ and 151° at $T = 0.27$. The two bubbles growing with time start to merge into one at $T = 0.51$, spanning from $\eta = 10°$ to 170°. At $\alpha = 45°$, the flow is no longer symmetric as previously stated. The flow starts to separate at $\eta = 165°$, $T = 0.19$. A second bubble develops much later at $T = 0.71$ at $\eta = 53°$, and at $T = 0.74$ merges with the first bubble, spanning from $\eta = 45°$ to 187°.

The time of separation decreases with Reynolds number as shown in Fig. 7. For $\mathrm{Re} > 10^5$, the separation time is essentially a constant, $T = 0.19$ for an elliptic cylinder with aspect ratio 0.6 and $\alpha = 0°$.

6.4. *Pressure Coefficient*

The pressure coefficient on the elliptic cylinder surface, Eq. (68), is evaluated for aspect ratio 0.6 and $\mathrm{Re} = 2500$ and plotted in Fig. 8 at angles of attack (a) $\alpha = 0°$, (b) $\alpha = 45°$, and (c) $\alpha = 90°$ for several times. Again the pressure is symmetric with respect to $\eta = 180°$ at $\alpha = 0°$ and with respect to $\eta = 90°$ at $\alpha = 90°$. At $\alpha = 45°$, the pressure distribution is no

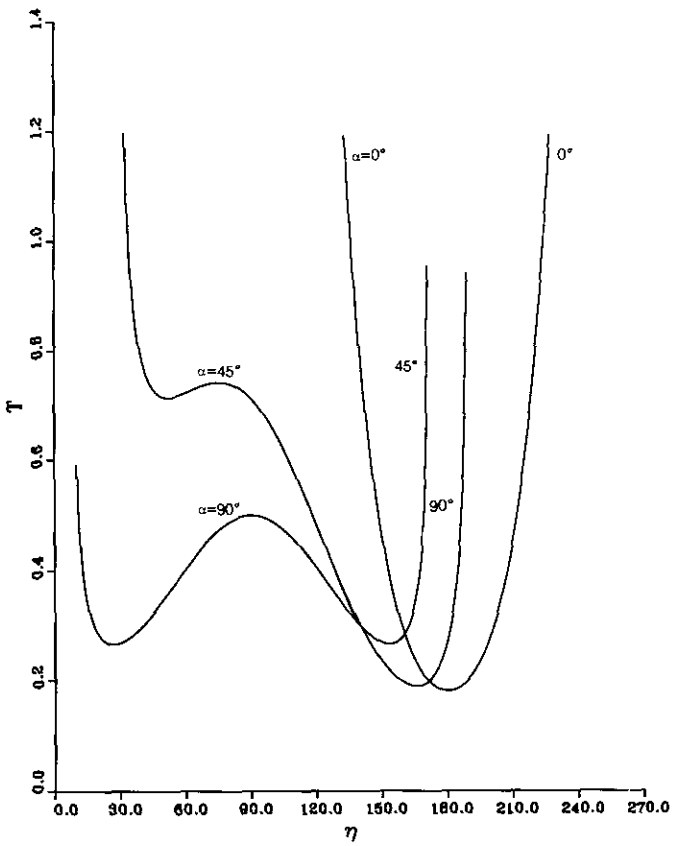

FIG. 6. Progression of the flow separation points for an elliptic cylinder with aspect ratio of 0.6, $\mathrm{Re} = 10^9$, and $\alpha = 0°$, 45°, and 90°.

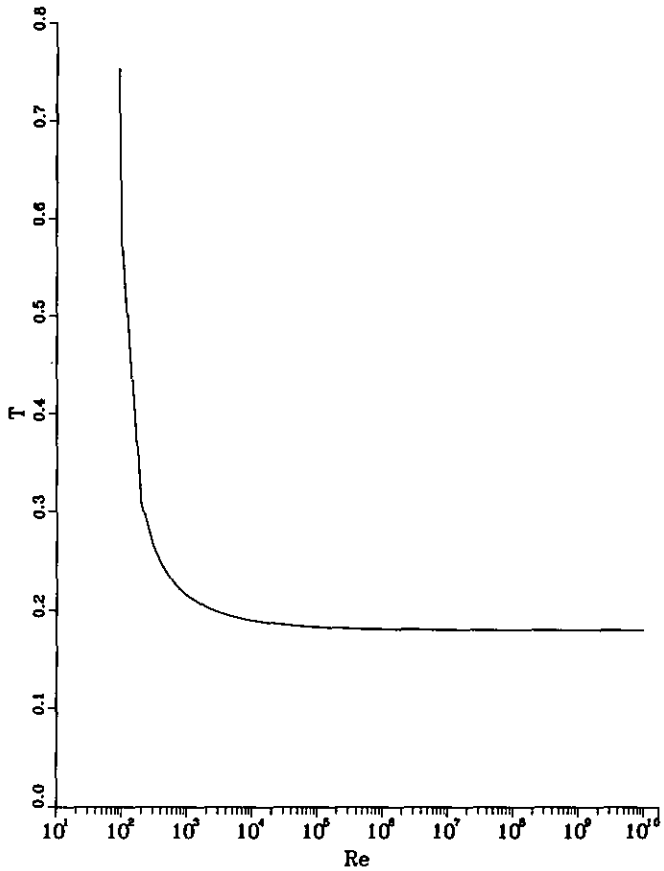

FIG. 7. Time of flow separation versus Reynolds number for an elliptic cylinder with aspect ratio of 0.6 and $\alpha = 0°$.

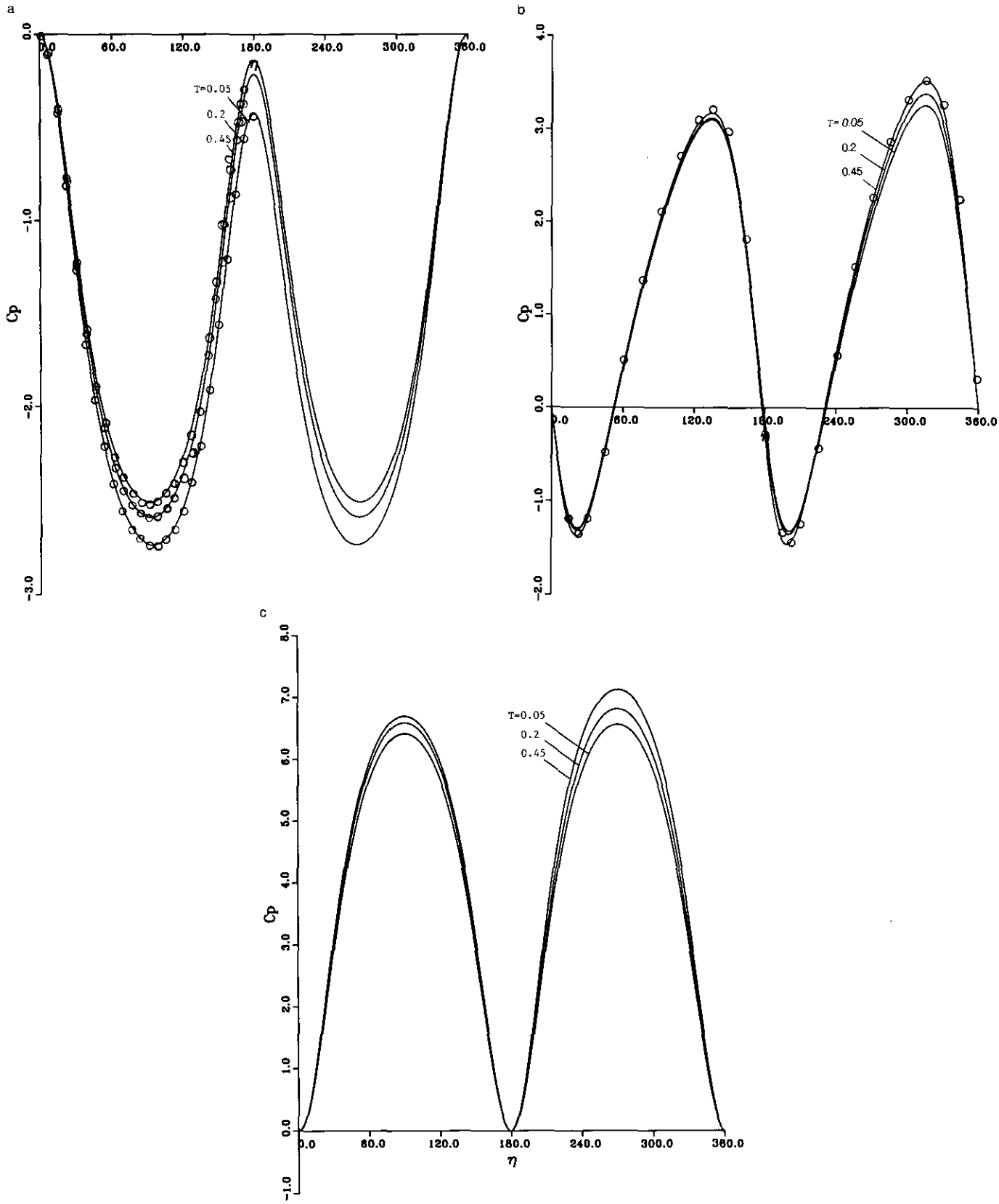

FIG. 8. Development of the surface pressure coefficient for an elliptic cylinder with aspect ratio of 0.6, Re = 2500; ○, Staniforth [10]: (a) $\alpha = 0°$; (b) $\alpha = 45°$; (c) $\alpha = 90°$.

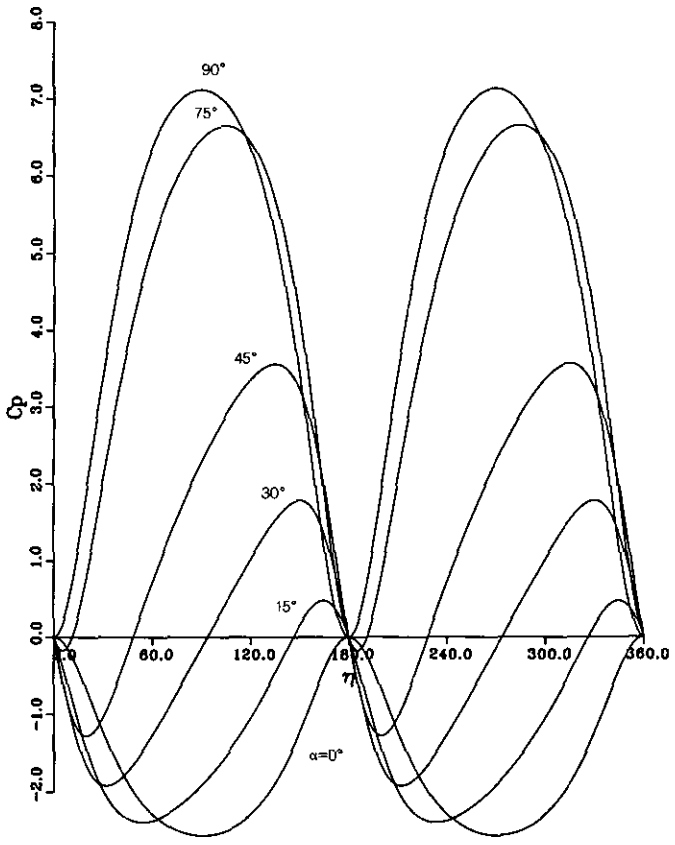

FIG. 9. Development of the surface pressure coefficient for an elliptic cylinder with aspect ratio of 0.6, Re = ∞, and $\alpha = 0°$, 15°, 30°, 45°, 75°, and 90°.

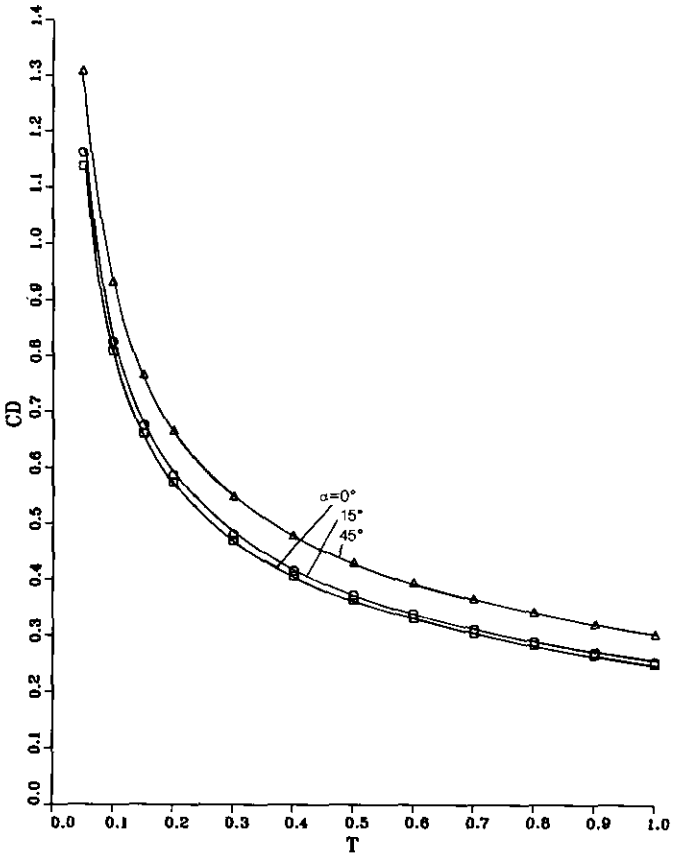

FIG. 10. Time history of drag coefficient for an elliptic cylinder with aspect ratio of 0.6, Re = 2500, $\alpha = 0°$, 15°, and 45°.

longer symmetric, with higher pressure on the windward side. The numerical computations of Staniforth, represented by open symbols, agree. The pressure coefficient, Eq. (69), for potential flow is the same as that for Re = ∞ plotted for six angles of attack in Fig. 9.

6.5. *Drag Coefficient*

The drag coefficient, Eqs. (70), for an elliptic cylinder with aspect ratio $b/a = 0.6$, at Reynolds number 2500, and angles of attack $\alpha = 0°$, 15°, and 45° are plotted in Fig. 10. Initially at $T = 0$, the cylinder experiences an infinite drag, which is due to the impulsive start of the cylinder. Kinetic theory may be required to explain the behavior of the flow at small time; see Yang and Lees [14].

6.6. *Lift Coefficient*

The corresponding lift coefficient, Eqs. (73), is plotted in Fig. 11. At $T > 0.6$, C_L becomes negative, which may be attributed to the fact that the present asymptotic solution is valid only for the small time. In fact, at larger Reynolds number, the lift is less negative. As in the case of the circular cylinder studied by the same method in Barlev and Yang [1], both lift and drag decrease with time which is assumed to be small. However, Staniforth's numerical computation shows that initially the lift and drag both decrease with time but then eventually start to increase with increasing time. At time zero, the lift coefficient also goes to infinity due to the impulsive nature of the flow.

7. CONCLUSION AND DISCUSSION

The impulsive, incompressible viscous flow past an elliptic cylinder has been studied by the method of matched asymptotic expansions to the third order, for which the pressure varies across the viscous layer. The outer flow has been shown to be irrotational, governed by the Laplace equation. The inner flow has been shown to be governed by the more complicated diffusion-type partial differential equations whose analytic solutions have been facilitated by the Symbolic Manipulation Program. A uniformly valid composite solution has been constructed from the outer and inner solutions. All of these solutions are valid for small times and large Reynolds numbers. However, the composite

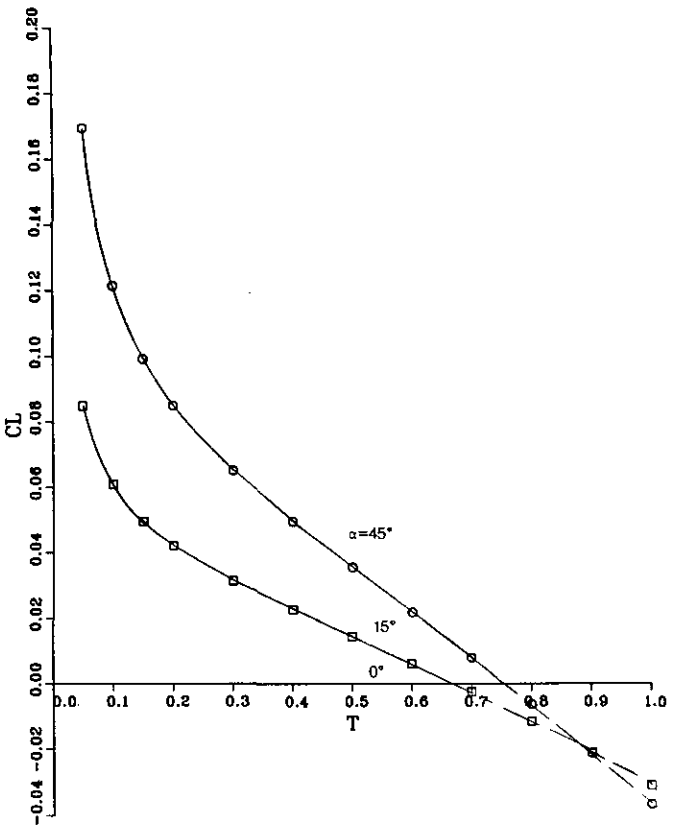

FIG. 11. Time history of lift coefficient for an elliptic cylinder with aspect ratio of 0.6, Re = 2500, $\alpha = 0°$, 15°, and 45°.

solution is too lengthy to be included; see Ref. [6] for details.

Numerical computations for the surface quantities such as the vorticity, the pressure distribution, the drag, and the lift coefficients were carried out for an ellipse of slenderness ratio 0.6 and Reynolds number 2500 in order to make comparisons with the numerical computations of Staniforth. The agreement in general is good. The discontinuity in Fig. 1 could perhaps be further studied by a third expansion.

ACKNOWLEDGMENTS

The senior author (H.T.Y.) is grateful to Professor H. K. Cheng for his interest and encouragement; Professor Milton Van Dyke for his critically constructive review and penetrating questions; Professor Larry Redekopp for reminding him about symmetry paradox, Mr. Dennis Plocher, Mr. Chor Tan, and Mr. Adam Fincham for helping in the contour plot, and Mr. Mark Michaelian for assistance as a merit scholar during 1987–1990; and Mr. Jerome Maes for his word-processing skills; last but most his parents for their sacrifices.

REFERENCES

1. M. Bar-Lev and H. T. Yang, *J. Fluid Mech.* **72**, 625 (1975).
2. D. F. Billings, Ph.D. thesis, University of Colorado, Boulder, 1984 (unpublished).
3. G. Birkhoff, *Hydrodynamics* (Princeton Univ. Press, Princeton, NJ, 1960), p. 38.
4. C. A. Cole and S. Wolfram, SMP (Symbolic Manipulation Program) Reference Manual, Version 1.6.0 (Inference Corporation, Los Angeles, 1987).
5. M. A. Goldshtik, "Viscous-Flow Paradoxes," in *Annual Review of Fluid Mechanics, Vol. 22*, (Annual Reviews, Inc., Palo Alto, CA, 1990), p. 456.
6. J. Hermel, Ph.D. thesis, University of Southern California, Los Angeles, 1984 (unpublished).
7. J. Kevorkian and J. D. Cole, *Perturbation Methods in Applied Mathematics* (Springer-Verlag, New York, 1985), p. 370.
8. L. M. Milne-Thomson, *Theoretical Hydrodynamics* (Macmillan Co., New York, 1968), p. 167.
9. L. Rosenhead, *Laminar Boundary Layers* (Clarendon Press, Oxford, 1963), pp. 121, 352.
10. A. N. Staniforth, Ph.D. thesis, University of Western Ontario, London, Canada, 1972 (unpublished).
11. M. Van Dyke, *Perturbation Methods in Fluid Mechanics* (Parabolic Press, Stanford, CA, 1975), p. 88.
12. C. Y. Wang, *J. Appl. Mech.* **89**, 823 (1967).
13. H. T. Yang, *Am. J. Phys.* **40**, 109 (1972).
14. H. T. Yang and L. Lees, *J. Math. Phys.* **35**, 195 (1956).